Synthesis and characterization of magnetic molecularly imprinted polymer nanoparticles for controlled release of letrozole

Saeedeh Kazemi*, Ali Asghar Sarabi**,†, and Majid Abdouss*,†

*Department of Chemistry, Amirkabir University of Technology, Tehran, P. O. Box 15875-4413, Iran
**Department of Polymer Engineering, Amirkabir University of Technology, Tehran, P. O. Box 15875-4413, Iran
(*Received 13 February 2016 • accepted 20 June 2016*)

Abstract−Synthesis and characterization of magnetic letrozole imprinted polymer nanoparticles is described herein for the first time. Magnetic molecularly imprinted polymers (MMIPs) were synthesized by precipitation polymerization using methacrylic acid (MAA) as functional monomer and trimethylolpropane trimethacrylate (TRIM) as cross-linker in the presence of letrozole as template and MAA-modified magnetite nanoparticles as magnetic component. The nanoparticles were characterized by scanning electron microscopy (SEM), transmission electron microscopy (TEM), X-ray powder diffraction (XRD), Fourier transform infrared spectroscopy (FT-IR), thermogravimetric analysis (TGA), and a vibrating sample magnetometer (VSM). The synthesized MMIP nanoparticles, with particle size of about 100 nm, showed superparamagnetic features with a saturation magnetization of 12.5 emu·g^{-1} and had thermal stability below 240 °C. The adsorption experiments indicated better template recognition of MMIP than magnetic non-imprinted polymer (MNIP) nanoparticles. Moreover, the release profile of letrozole from MMIP and MNIP revealed the controlled release ability of MMIP nanoparticles for the letrozole anticancer drug. We also found that applying an external alternative magnetic field results in increasing the rate of the drug release.

Keywords: Molecularly Imprinted Polymer, Adsorption Capacity, Magnetite Nanoparticles, Letrozole, Drug delivery

INTRODUCTION

Controlled drug delivery systems have attracted considerable attention and dramatic changes are anticipated in the near future. These systems can target the drug at specific sites of the body (organ, tissue, cell or tumor) or they can regulate the rate or the amount of the therapeutic agent release. Some controlled delivery systems have both capabilities at the same time. These features lead to the reduction of adverse side effects, preventing the drugs from attacking the healthy parts of the body, maintaining the desired therapeutic level and avoiding high-dose administration of the drug. These capabilities are especially important for cytotoxic anticancer drugs [1-4]. Molecular imprinting polymers are one of the promising materials for developing controlled drug delivery systems [5-10].

Molecular imprinting technology provides smart polymers which have recognition sites complementary to a target molecule called a template. Forming complexes between the template and monomers during the polymerization step leaves cavities in the obtained polymer network, which matches the template in size, shape and functional groups. After the template is removed with suitable solvents, the cavities act as a specific binding site that selectively rebinds the template. Selective recognition and template affinity along with an easy and low cost preparation, stability against organic solvents and unfavorable conditions (such as thermal, mechanical and pH changes) [11-13] have attracted considerable attention to MIPs in a wide area of applications such as solid-phase extraction [14], liquid chromatography [15], membrane technology [16], sensors [17] and biosensors [18], enantio-selective recognition and separation [19], enzyme-like catalysts [20,21] and pharmaceutical applications, such as drug discovery [22], drug purification [23] or drug delivery [24,25].

Due to the affinity of the template for the functional groups in the binding sites of the MIP network, the release rate of the template decreases. Therefore, MIPs can be used to develop sustained-release drug delivery systems. By controlling the amount and type of the monomers and cross-linker agents, the release rate of a therapeutic agent, used as the template, can be regulated [23,26,27]. Moreover, stimuli-responsive MIPs can help to design a targeted delivery system that releases a template in response to a specific stimulus such as changes of pH, temperature, incident light, ionic strength or even the presence of a specific molecule at the desirable site or even on the surface of a tissue or cell [5,24,28,29].

In recent years, a simple and effective method has been developed for synthesis of a targeted delivery system based on combining the magnetic properties of magnetite nanoparticles [30-32] with molecular imprinting polymer technologies. These magnetic molecularly imprinted polymers (MMIPs) can be localized to a targeted site by responding to the external magnetic field in order to increase the concentration of the magnetic MIP nanoparticles and the release of the drug in the targeted area. Additionally, magnetic MIPs have an advantage compared to common MIPs. These polymers can separate easily and rapidly in the preparation and synthesis process without wasting any materials and time to separate polymers with the centrifugation or filtration process [33-36].

†To whom correspondence should be addressed.
E-mail: sarabi@aut.ac.ir, phdabdouss44@aut.ac.ir

Letrozole (Femara®) is a non-steroidal, highly selective aromatase inhibitor used in the treatment of postmenopausal women with an early-stage or advanced, hormone-sensitive (responsive) breast cancer. The inhibition of aromatase activity prevents converting androgens to estrogens in the peripheral tissues. Reduction of whole body aromatization and aromatase activity in breast tumors, and plasma levels of estrone, estradiol and estrone sulfate were seen with letrozole in postmenopausal women with breast cancer [37-39]. However, similar to other cytotoxic drugs, patients suffer from adverse side effects of letrozole treatment. Common side effects of letrozole include hot flashes, hair loss, pain in the joints, bones and muscles, tiredness, unusual sweating or night sweats, nausea, diarrhea, dizziness, trouble sleeping, drowsiness, weight gain, weakness, headache, constipation and numbness, tingling, weakness and stiffness in hand or fingers [40-42].

Until now, few studies focused on developing a controlled drug delivery system to decrease the adverse side effects of letrozole [43-45], and no research has been reported on the magnetic carriers or molecular imprinted polymers for this anticancer drug. In the present work, we synthesized and evaluated a controlled drug delivery system based on the magnetic molecularly imprinted nanoparticles for the letrozole. The Fe_3O_4 magnetic nanoparticles (MNPs) were synthesized by the co-precipitation technique and functionalized with MAA by a simple complexing reaction. Then the MMIP was synthesized using MAA as functional monomer, TRIM as cross-linker, letrozole as template and MAA-modified magnetite nanoparticles as magnetic component. The nitrogen atoms of the letrozole can be bound to the functional groups of monomers with non-covalent interactions, which are favorable interactions for the binding/rebinding processes required to incorporate and release the templates. MMIP nanoparticles were characterized by scanning electron microscopy (SEM), transmission electron microscopy (TEM), X-ray powder diffraction (XRD), Fourier transform infrared spectroscopy (FT-IR), thermogravimetric analysis (TGA) and a vibrating sample magnetometer (VSM). Several adsorption experiments were carried out to evaluate the recognition properties of MMIP. Release experiments were also performed to investigate the ability of the synthesized MMIP for drug delivery applications. Additionally, the effect of applying an alternative magnetic field on the release behavior was studied.

EXPERIMENTAL

1. Materials

Methacrylic acid (MAA), 2,2′-azoisobutyronitrile (AIBN), disodium hydrogen phosphate, sodium dihydrogen phosphate, iron(II) chloride tetrahydrate ($FeCl_2 \cdot 4H_2O$), iron(III) chloride hexahydrate ($FeCl_3 \cdot 6H_2O$), and ammonium hydroxide (NH_4OH) were purchased from Merck (Darmstadt, Germany) and 1,1,1-trimethylolpropane trimethacrylate (TRIM) was prepared from Sigma-Aldrich (Sigma Chemical Co., St Louis, MO, USA). The letrozole template was prepared from Iran Hormon Company, Iran, and the miconazole powder was prepared from Behvazan pharmaceutical Company, Iran.

2. Instruments and Apparatus

Fourier transform infrared (FT-IR) spectra of the nanoparticles

were recorded in the range of 400-4,000 cm^{-1} using a Bruker Equinox 55 spectrometer with KBr pellet.

The structure of the synthesized Nanoparticles was characterized by X-ray diffractometer (XRD, Inel Equinox 3000, France). The x-ray diffraction patterns were taken from 20 to 80 (2θ value) using Cu Kα radiation (λ=1.541874 A).

Magnetic properties were measured with BHV-55 (Riken, Japan) vibrating sample magnetometry (VSM) in a field range up to 10 kOe.

The concentrations of the letrozole in the solutions were detected by a UV-Vis Jenway 6505 spectrophotometer. The morphology of the synthesized nanoparticles was characterized using field emission scanning electron microscopy (FE-SEM) in a Zeiss instrument (Germany) and the transmission electron microscopy (TEM) on a LEO 906, (Germany) TEM microscope.

Thermogravimetric analysis (TGA) was also performed on a Mettler-Toledo TGA-1 (Switzerland) from room temperature to 800 $^\circ$C with a heating rate of 10 $^\circ$C·min^{-1} under nitrogen flow.

The magnetic field was generated by an external alternating magnetic field (AMF) apparatus (Electromagnet Type E, England).

3. Preparation of Magnetite Nanoparticles

The Fe_3O_4 MNPs were prepared by the co-precipitation technique according to the following method: 2.5 g $FeCl_3 \cdot 6H_2O$ and 0.919 g $FeCl_2 \cdot 4H_2O$ were dissolved in 25 mL of de-ionized water and then degassed by pulse mode in an ultrasonic bath. Then 250 mL of aqueous solution containing 7 mL of ammonium hydroxide (25%, w/v) was prepared and purged with N_2 gas. Iron salts were added to this solution drop by drop in 10 min while stirring vigorously. The reaction was maintained for 40 minutes at 25 $^\circ$C under N_2 atmosphere. The black precipitate was collected with a strong magnet and washed several times by ethanol and distilled water until the pH of the suspension reached to pH 7. The precipitate was then dispersed in ethanol and purged with N_2 gas to prevent oxidation, for further applications.

4. Synthesis of Magnetic Molecularly Imprinted Polymer Nanoparticles

The precipitation polymerization technique was used for the preparation of MMIP according to the following procedure. First, 3 mmol of MAA was dispersed in 20 mL of suspension containing 200 mg of MNP by ultrasonic waves for 20 min. The suspension was then stirred at 40 $^\circ$C for 18 h to functionalize the surface of MNP with MAA. The resulting product was washed with ethanol and acetone several times and dispersed in 30 mL of acetonitrile solution in a 75 mL glass flask. Then 2 mmol of the letrozole template and 3 mmol of MAA were added and the mixture was stirred at 100 rpm for 2 h to form a template-monomer complex. After that, 2 mmol TRIM and 20 mg AIBN were added and the polymerization components were mixed by an ultrasonic wave for 15 min. The flask was purged with a gentle flow of nitrogen gas for 5 min and was sealed under nitrogen, and the reaction was allowed to proceed in a water bath at 60 $^\circ$C for 24 h in order to form Magnetic MIP. The obtained polymers were separated by the external magnetic field and washed with ethanol and acetone to remove all the impurities. The product was washed with a mixture of methanol and acetic acid (9 : 1 v/v) until the complete removal of the template molecules was confirmed by UV-Vis spectroscopy and

then washed with ethanol and acetone. Furthermore, magnetic non-imprinted polymers (MNIP) were prepared, as a blank, using the same synthesis process without the addition of the template molecule. MMIP and MNIP were dried in a vacuum oven at 40 °C for 18 h.

5. Adsorption Experiments

Adsorption experiments were carried out to investigate the amount of template bound to the polymer and selectivity of the MIP materials. The amount of template bound to the polymer can be expressed in two ways, including the adsorption capacity Q (mg·g^{-1}) and the percent of extracted template from the solution containing standard concentration of template (% extracted template).

For the determination of the amount of template bound to the polymer, 50 mg of the MMIP and MNIP samples was added to 10 mL suspension of 50 mg·L^{-1} letrozole in methanol. The suspension was gently agitated by shaking the bottles in a horizontal position at around 100 rpm on a shaker at room temperature for 24 h. The polymers were separated from the suspension by the external magnetic field and then centrifuged for 10 min (10,000 rpm) and the concentration of the letrozole in the liquid phase was measured by UV-Vis spectrometry at λ_{max}=240 nm.

The adsorption capacity Q (mg·g^{-1}) and the % extracted template were calculated according to Eq. (1) and Eq. (2).

$$Q = \frac{(C_i - C_f)}{M} \times V \qquad (1)$$

$$\% \text{ Extracted Template} = \frac{(C_i - C_f)}{C_i} \times 100 \qquad (2)$$

where C_i and C_f (mg·L^{-1}) are the initial concentration and the residual concentration of letrozole, respectively; V (liter) is the initial volume of the solution; and W (grams) is the weight of the MMIPs or MNIPs.

Based on above experiments, adsorption capacity (Q) and the % extracted template in eight different concentrations were calculated (0-100 mg·L^{-1}). The initial concentration for letrozole solution with calculated adsorption capacity Q and % extracted template, corresponding to each concentration are shown in Table 1.

A calibration curve was recorded by using five different letrozole standard solutions and a correlation coefficient (R^2); the slope and intercept of the regression equation were obtained by the method of least square.

With the aim to evaluate the selectivity of MMIPs to letrozole, the same binding experiments were performed using 10 mL suspension of 50 mg·L^{-1} of miconazole that is structurally similar to letrozole.

6. In Vitro Release of Letrozole

For investigation of in vitro release behavior of synthesized nanoparticles, 100 mg of MMIP and MNIP samples was loaded with letrozole solution and then separated by an external magnetic field and dried under vacuum. The letrozole-loaded nanoparticles were dispersed in flasks containing 50 mL of phosphate buffer solution (0.1 M, pH 7.4, simulating biological fluids). The entire system was kept at 37 °C by gently shaking throughout the experiment. For studying the influence of magnetic field on the release rate, the mentioned system was kept between magnetic poles of an external alternating magnetic field apparatus for 240 min. Magnetic field frequency was 350 kHz and the strength of the magnetic fields (150 and 300 G) was changed by adjusting the voltage of the equipment. To characterize the released drug, 3 mL of samples were drawn from the suspension at designated time intervals, and the same volume of fresh medium was added to the medium. The percentage of the released letrozole at each moment of the experiment was determined by UV-Vis analyses.

RESULTS AND DISCUSSION

1. Synthesis and Characterization of MMIP and MNIP

Magnetic molecularly imprinted polymers were synthesized using the procedure described in Fig. 1. The template-monomer complexes were created in pre-polymerization process as a result of the interactions between letrozole template and MAA monomers. Then precipitation polymerization was performed using MAA as functional monomer and TRIM as cross-linker in the presence of letrozole template and MAA-modified magnetite nanoparticles.

The interactions between functional monomers and template molecules during polymerization leave cavities in the obtained polymer. These cavities act as specific binding sites that can selectively bind or rebind to the template through the interactions between functional groups in the template molecule and polymer matrix. Mainly, these interactions are covalent or non-covalent interactions. Since the non-covalent interactions lead to fast kinetics of binding, these types of interactions are favorable for binding/rebinding process required to incorporate and release the template. Moreover, although non-covalent interactions are relatively weak, they allow binding with strong affinities between template and monomers. Also, non-covalent interactions benefit from other advantages; for example, simple reaction to create template/monomer complexes in the pre-polymerization process, easy removal of the template with washing without any need for chemical cleavage like covalent imprinting [11-13]. In this research, the carboxylic acid groups of MAA were used to create hydrogen interactions between the polymer matrix and the nitrogen atoms of the letrozole ring (Fig. 1). The interactions between letrozole and MAA were studied in a computational work that was previously published by our team, which the results indicated forming interactions between nitrogen atoms of the letrozole ring and the hydrogen atoms of
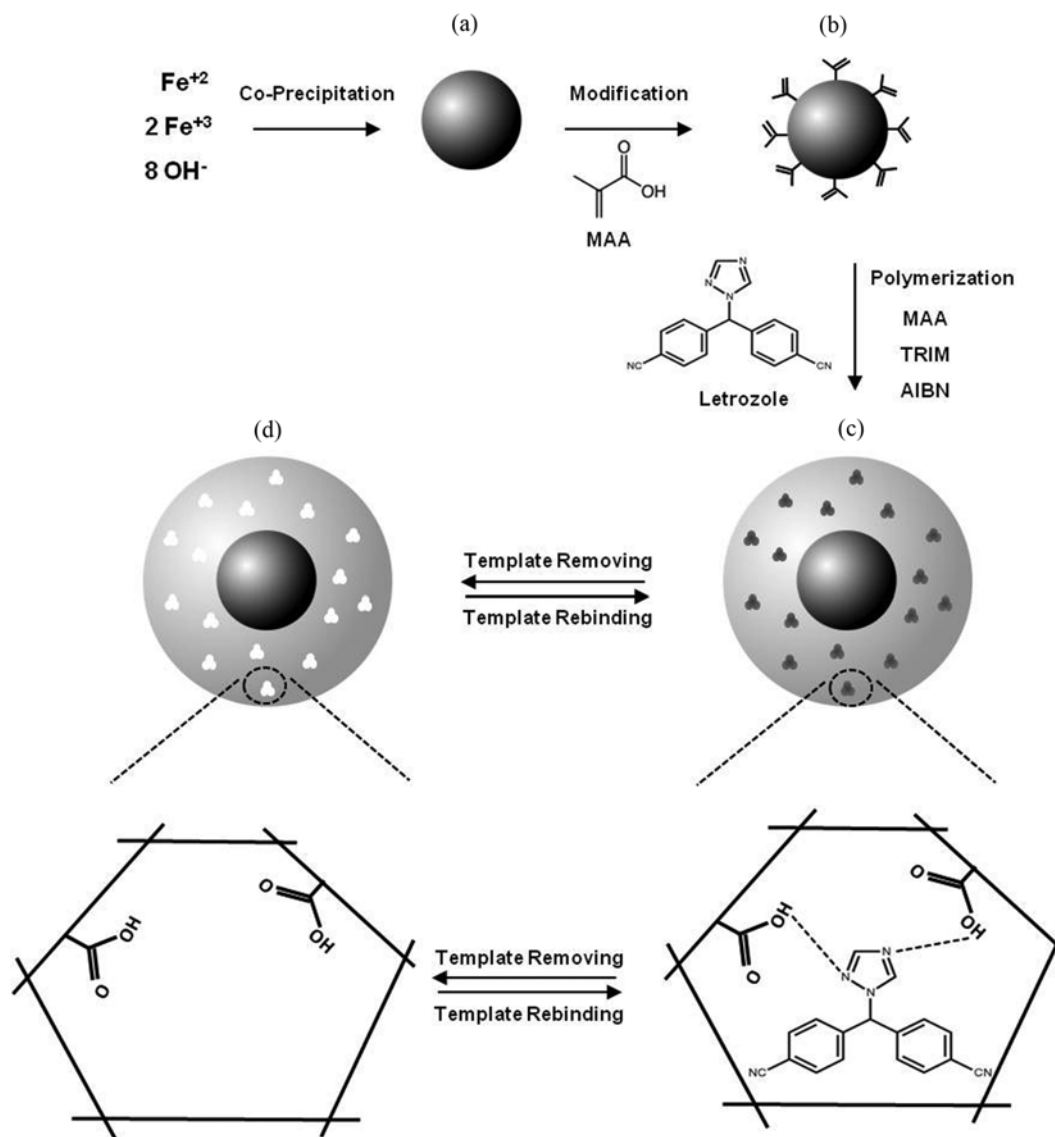
Table 1. Adsorption capacity (Q) and % extracted template (%Ex) versus initial template concentration (C_i)

C_i	MMIP		MNIP	
	Q	% Ex	Q	% Ex
5	0.78	78	0.6	60
10	1.62	81	1	50
15	2.5	83.33333	1.4	46.66667
25	4.3	86	2.6	52
35	6.24	89.14286	3.6	51.42857
50	9.2	92	5.4	54
75	11.4	76	7.4	49.33333
100	12	60	8.2	41

Fig. 1. Schematic representation of magnetic letrozole imprinted polymer nanoparticles synthesis process. (a) Fe₃O₄ MNP, (b) MAA-modified MNP, (c) MMIP and (d) template removed MMIP.

carboxylic acid group of MAA [46].

The morphology of the synthesized samples was characterized using scanning electron microscopy (SEM) and the transmission electron microscopy (TEM). The SEM and TEM images of the MNP and MMIP are shown in Fig. 2. These images reveal that the obtained Fe_3O_4 nanoparticles have spherical morphology and a diameter less than 20 nm. Due to their small size, these nanoparticles agglomerate easily. MMIP nanoparticles have an average particle size of about 100 nm. As the polymers were obtained from the precipitation polymerization, the resultant products resembled in size and shape, which is an important factor for drug delivery applications [47].

The XRD pattern and FT-IR spectra of the Fe_3O_4 MNP and MMIPs confirmed the existence of the magnetite structure in all of the synthesized samples.

The x-ray powder diffraction spectra of the MNP and MMIP are shown in Fig. 3. Characteristic peaks were observed in the

XRD pattern at 2θ of 30°, 35°, 43°, 53°, 57° and 62° corresponding to the diffractions of (220), (311), (400), (422), (511), (440), respectively (JCPDS Card: 19-629) [33,48]. This result indicated the existence of Fe_3O_4 structure in three samples without any changes after the polymerization process. In comparison with the bare magnetite, the two other samples showed a reduction of peak intensity. This could be due to the lower magnetite content in MMIP and MNIP that has a polymeric shell on the surface [49].

Functionalization of the magnetite nanoparticles was implemented by a simple method previously used by other researchers as well. In 2011, Zhang and his coworkers used a simple coordination reaction method for modification of the magnetite with acrylic acid and proved their claim by FT-IR spectra of magnetite nanoparticles before and after the modification. The presence of a vibration band of C=O stretching confirmed successful modification of the acrylic acid monomer [50]. Also, Zhou et al. used a similar method for surface modification of the magnetite with MAA. They
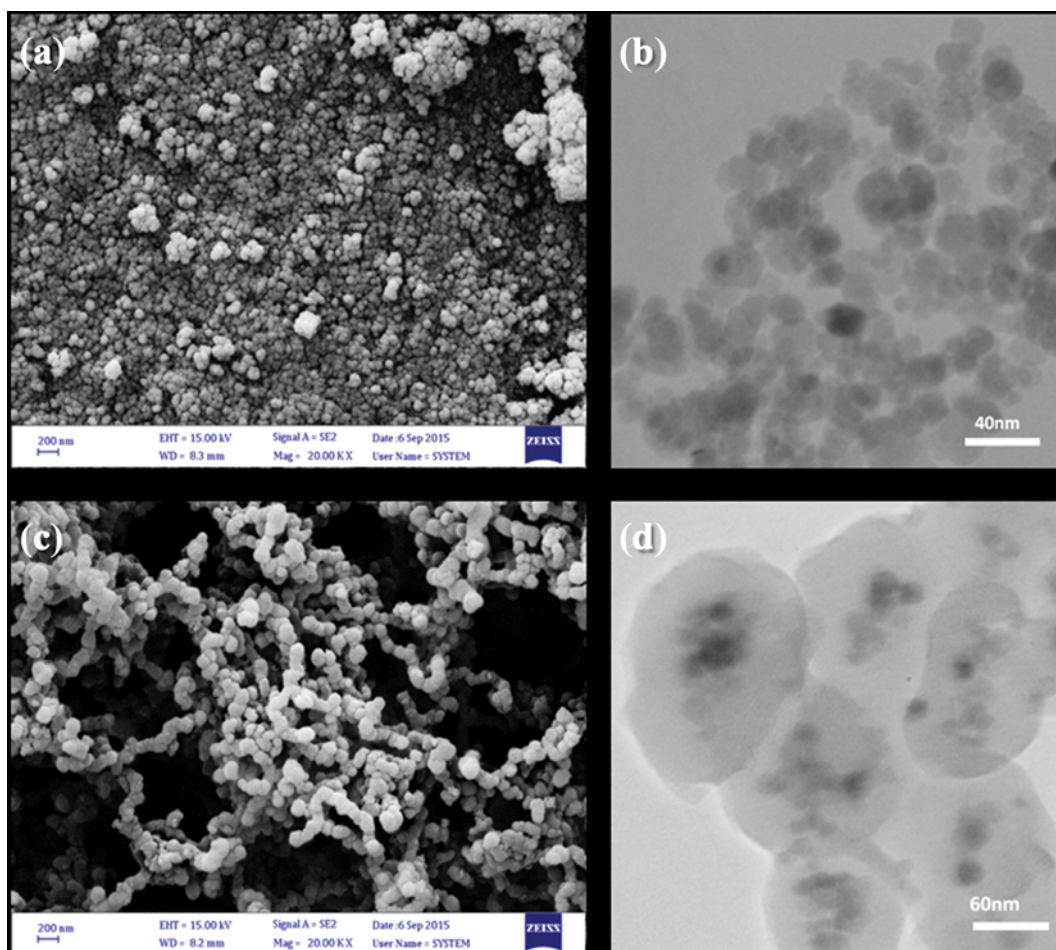
Fig. 2. SEM and TEM micrographs of nanoparticles. (a) SEM image of Fe$_3$O$_4$ MNP, (b) TEM image of MMIPs, (c) SEM image of Fe$_3$O$_4$ MNP and (d) TEM image of MMIPs.
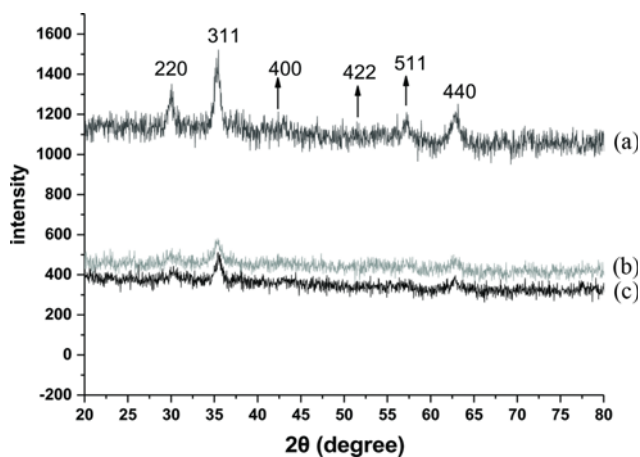

Fig. 3. XRD patterns of (a) Fe$_3$O$_4$ MNP, (b) MMIP and (c) MNIP.

confirmed grafting of MAA onto the magnetite surface by the presence of a peak at 1,635 cm^{-1} in the FT-IR spectra of the MAA-modified nanoparticles, belonging to the C=C stretching vibrations [51].

The FT-IR spectra for MNP (a), MAA-modified MNP (b),

MMIP before and after the elution step ((c) and (d)) and MNIP (e) are shown in Fig. 4. The presence of the characteristic absorption band of Fe-O, around 590 cm^{-1} in all spectra demonstrated the existence of Fe$_3$O$_4$ MNPs in the structure of all samples. The peak weakened in the spectra of MMIP and MNIP due to coating of magnetite with a poly (methacrylic acid) shell [50,52]. Spectra of MAA-modified MNP are shown in Fig. 4 curve b. In comparison with MNP spectra (a), two assignable peaks were added. The peak at 1,637 cm^{-1} was attributed to C=C stretching vibrations of MAA monomers and the peak at 1,700 cm^{-1} corresponded to the C=O group of MAA. This observation demonstrated successful modification of magnetite nanoparticles with MAA [50,51]. A broad band at 3,424 cm^{-1} was visible in all five spectra, which was attributed to the stretching frequency of the -OH bond of the water and the surface hydroxyl groups of the MNP, MAA and polymers. The peaks of the -CH$_2$ and -CH$_3$ stretching vibrations were located around 2,965 cm^{-1}. -CH$_2$ and -CH$_3$ bending vibrations were seen at 1,386 and 1,460 cm^{-1}. C-O symmetric and asymmetric stretching vibrations of ester corresponded at peak 1,260 and 1,148 cm^{-1}. A strong peak at 1,737 cm^{-1} was observed in all of the spectra attributed to the characteristic ester carbonyl stretching bond. The presence of the mentioned vibrations proved the formation of
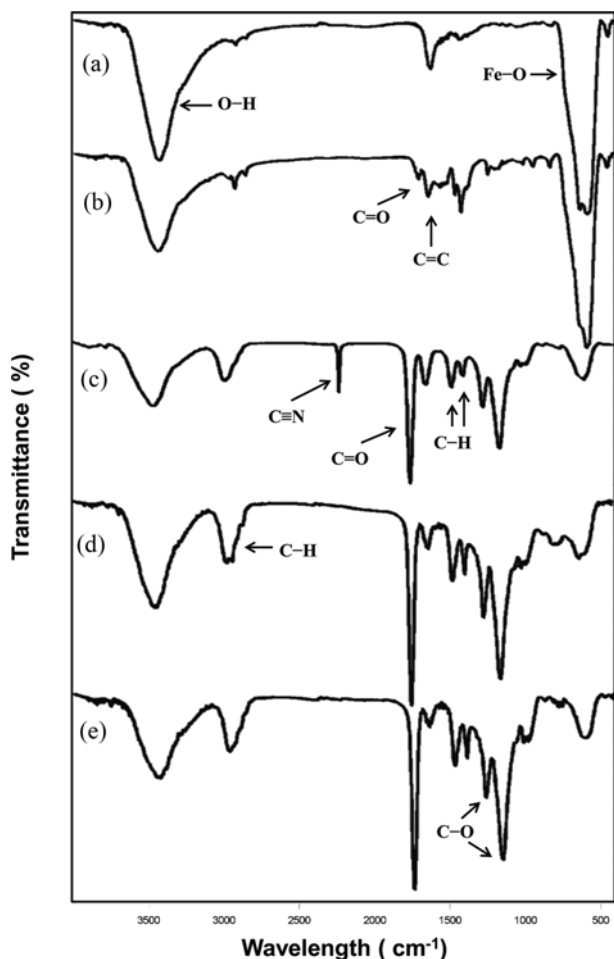
Fig. 4. FT-IR spectra of (a) Fe$_3$O$_4$ MNP, (b) MAA-modified MNP, (c) MMIP before elution step, (d) MMIP after elution step and (e) MNIP.

a polymeric shell on the MNP surfaces in the structure of the MMIPs and MNIP as a result of the cross-linking process between MAA and TRIM [53]. The main difference between spectra c, d
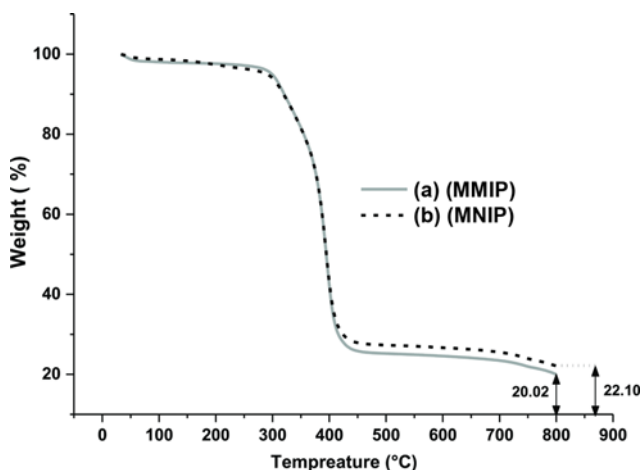
and e was due to the appearance of a band at 2,230 cm^{-1} in the spectra of un-leached MMIP, ascribable to the C≡N bond, which was absent in the leached MMIP and MNIP. This fact indicated the removal of the letrozole template after the elution step in MMIP and also pointed to no essence of template in the NIP nanoparticles.

The thermogravimetric analysis (TGA) of the MMIP and MNIP samples is shown in Fig. 5. Samples showed a lower than 2% weight loss at the temperatures less than 150 °C, which was mainly due to the moisture evaporation caused by inadequate drying. There was no dramatic weight loss below the temperature of 250 °C. Significant mass loss began from 300 to 445 °C, which was attributed to the decomposition of the Poly (methacrylic acid) [54]. The remaining mass was attributed to the thermal resistance of Fe$_3$O$_4$ nanoparticles, which cannot be melted until 1,594.5 °C. The quantity of Fe$_3$O$_4$ particles in the samples was 20.02% for MMIP and 22.10% for MNIP, respectively. Regarding the equal amount of magnetite applied in the synthesis processes, the lower weight percentage of the remaining magnetite in the MMIP was attributed to the presence of the template in its structure [55].

The magnetic properties of MNP and MMIP nanoparticles were investigated with a vibrating sample magnetometer (VSM) and hysteresis curves are shown in Fig. 6. Both samples illustrated superparamagnetic behavior, as they had no coercivity (the field required to bring the magnetization to zero) and no remnant magnetization [56,57]. If the nanoparticles' size is less than a critical value (25 nm), each particle turns into a single magnetic domain and behaves like a giant paramagnetic atom that has a fast magnetic response time and negligible remanence and coercivity. Thus, the results represented the small particle size of MNPs. The saturation magnetization value was measured to be 60 emu·g^{-1} for MNP and 12.5 emu·g^{-1} for MMIP. The high saturation magnetization of pure Fe$_3$O$_4$ indicated a good crystal structure. The magnetization value for MMIP was smaller than that for MNP, which was due to the existence of a polymeric coating on the surface of the magnetite nanoparticles. As the polymeric shell is diamagnetic, it quenches the magnetic moment. However, MMIP still showed superparamagnetic behavior due to the existence of magnetite nanoparticles
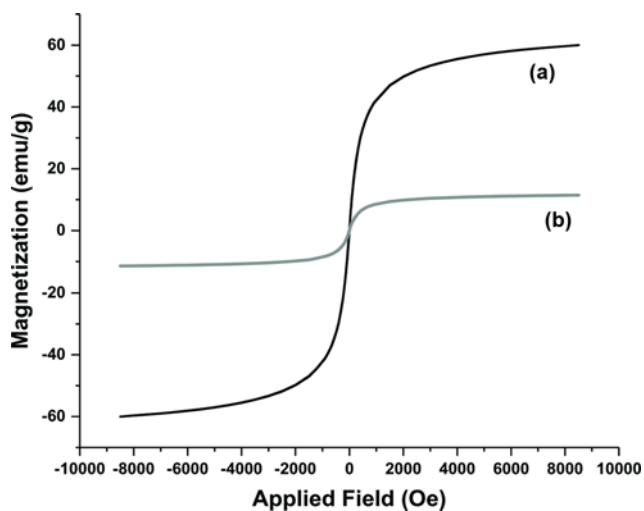

Fig. 5. Thermogravimetric analysis of (a) MMIP and (b) MNIP.

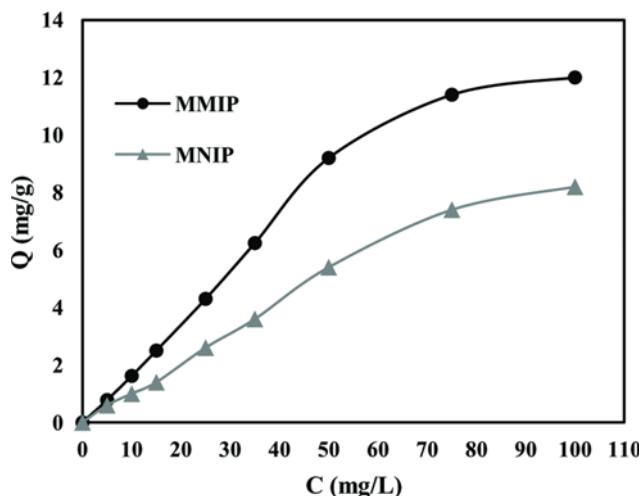**Fig. 6. Magnetization curves of (a) Fe$_3$O$_4$ MNP and (b) MMIP.**

Fig. 7. Adsorption isotherm of MMIP (●) and MNIP (▲) at temperature 37 °C.

in its structure [58]. This is while MMIP showed enough magnetic response to be controlled by an external magnetic field. The magnetic responses of MNP and MMIP were tested by placing a magnet near the glass bottles. Both powders were attracted by the magnet, but separation of the MNP powder from the emulsion needed less time.

2. Imprinting Properties

The imprinting properties of magnetic MIPs were evaluated by the adsorption isotherm and the % extracted template in which the amounts of polymeric nanoparticles were incubated with different concentrations of letrozole solution for 24 h. The adsorption isotherm curve is shown in Fig. 7. For both MMIP and MNIP samples, the amounts of the adsorption capacities increased with increasing of the letrozole concentration in the solution. Also, magnetic MIPs showed higher adsorption capacity than MNIPs in all concentrations. The adsorption capacity and % extracted template versus initial template (letrozole) concentration are shown in Table 1. Magnetic MIPs showed higher amount for % extracted template than MNIPs in all concentrations. Also, the highest percent-
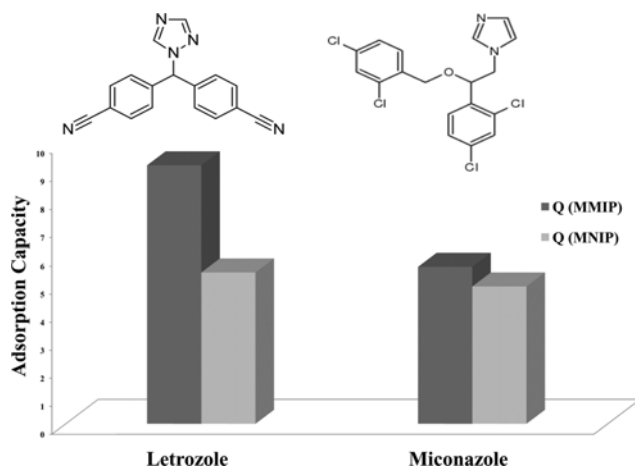
age of template extraction was observed in the initial concentration of 50 mg·mL^{-1}.

For the evaluation of the selectivity, the adsorption capacity was evaluated for polymeric nanoparticles incubated in the letrozole and miconazole solution (50 mg·mL^{-1}) and the results are compared in Fig. 8. For MMIP the adsorption capacity of letrozole is higher than that for miconazole, whereas, there are no significant differences between the adsorption capacity of letrozole and miconazole for MNIP. Higher adsorption capacity for letrozole than miconazole indicated good selectivity of MMIP for letrozole.

The imprinting efficiency (α) represents an easy way to highlight the recognition properties of imprinted materials and it is defined as the ratio of adsorption capacities between the MMIPs and MNIPs (Eq. (3)).

$$\alpha_{imprinting\,factor} = \frac{Q_{MMIP}}{Q_{MNIP}} \tag{3}$$

The imprinting factors of letrozole and miconazole were calculated as 1.7 and 1.1, respectively. As was mentioned for adsorption capacity, higher imprinting factor of the MMIP for letrozole compared with miconazole represented good selectivity of synthesized MIP for template. Higher adsorption capacity and selectivity of MMIP than MNIP are attributed to the existence of the letrozole in the synthesis process.

The presence of the template in the polymerization step for MIP materials leads to forming specific binding cavities in the polymeric matrix that match with the configuration and functional group of the template molecule. Thus, interactions between MIP and the special template are better compared with NIP [34].

3. In Vitro Drug Release

The *in vitro* release profile for letrozole from the magnetic imprinted and non-imprinted nanoparticles at 37 °C in a buffer solution (pH 7.4) is shown in Fig. 9. As it was observed, about 40% of the total loaded letrozole was released during 10 h from the imprinted matrix, while about 80% of the loaded letrozole was released within the same time from the MNIP. The drug was completely released within 20 h and 70 h by MNIPs and MMIPs, respectively. The absence of the template in the polymerization step for MNIP
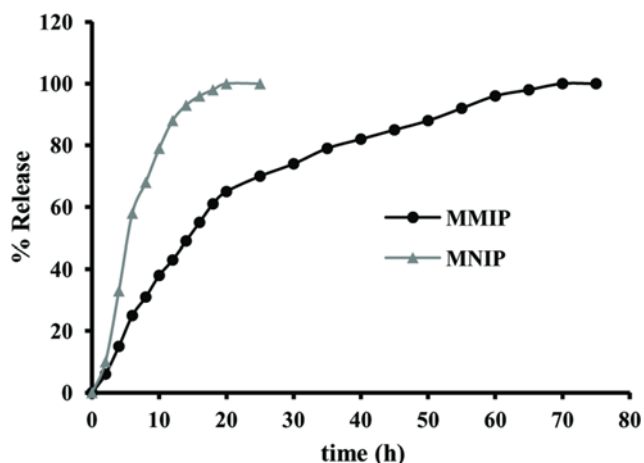

Fig. 8. Adsorption capacity of MMIP and MNIP.

Fig. 9. Release profile of MMIP (●) and MNIP (▲) at 37 °C in a buffer solution (pH 7.4).

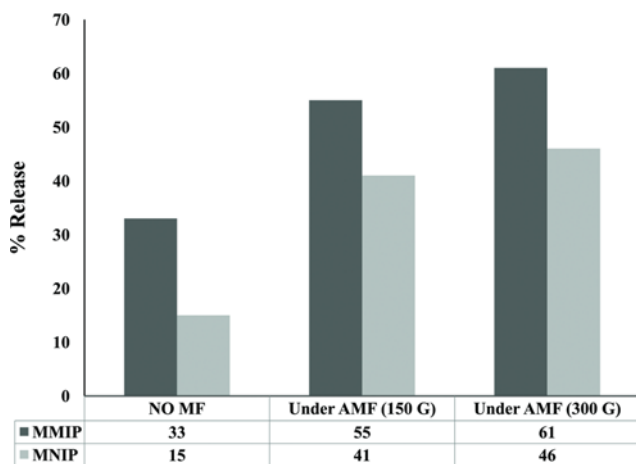|	NO MF	Under AMF (150 G)	Under AMF (300 G)
■ MMIP	33	55	61
■ MNIP	15	41	46

Fig. 10. Influence of Alternative magnetic field on the release behavior of MMIP and MNIP in a buffer solution (pH 7.4).

leads to forming a non-specific bound between template and monomer that consists of the main interactions in this polymer. However, the specific cavities for the template in the MMIP matrix lead to strong template-monomer interactions [26]. For both MMIP and MNIP nanoparticles, we saw a quick release in the initial period that was related to physically adsorbed drug molecules at the surface of the polymers and releasing from non-specific binding sites. However, for MMIP, this rapid release slowed down and drug release was continued by the sustained profile that attributed to the release from specific binding sites [33,59]. So MMIPs showed a controlled release profile for letrozole and lasted a long time for drug release compared with non-imprinted nanoparticles. This observation represented better specificity of MMIP compared with MNIP, which was in agreement with the results of imprinting experiments and adsorption isotherm.

The influence of an alternative magnetic field on the drug release behavior was also investigated, and the results are shown in Fig. 10. After 240 min of exposure to AFM, with the strengths of 150 and 300 G, at 37 °C in a buffer solution (pH 7.4), the amount of the released drug was calculated. As seen in the figure, the amount of the drug released increased under AFM. Compared with the release amount with no magnetic field, MMIP indicated 22% and 28% more release of letrozole, respectively. A similar increasing was observed for MNIP release rate under AFM. The possible reason for such an increase in the drug release upon application of the magnetic field is that applying an alternative magnetic field increases the agitation and motion of the magnetic nanoparticles, which leads to the formation of more open structures in the polymer matrix. This change in polymer structure allows the drug to be released more easily. These findings are in agreement with the results that have previously been published [60-63].

CONCLUSION

Magnetic MIP nanoparticles were synthesized by the precipitation polymerization of MAA and TRIM in the presence of letrozole as template and MAA-modified magnetite nanoparticles as magnetic agents. The obtained MMIP nanoparticles were charac-terized by FE-SEM, TEM, FT-IR, XRD, VSM and TGA. The adsorption experiments indicated that MMIPs have good recognition properties and selectivity for letrozole. The *in vitro* drug release experiment showed that MMIPs have more sustained-release properties compared with MNIP, which represents their higher affinity to the template. It was also found that the amount of the released drug from MMIP and MNIP increased by applying an alternative magnetic field. Moreover, due to the superparamagnetic behavior of the synthesized MMIP nanoparticles, which was approved by VSM, they can be conducted to the target tumor in the body by the aid of an external magnetic field, in order to decrease the letrozole side effects on the healthy organs. We believe that the synthesized magnetic imprinted nanoparticles are promising tools for application in targeted and sustained-release drug delivery.

REFERENCES

1. X. Xu, W. Ho, X. Zhang, N. Bertrand and O. Farokhzad, *Trends Mol. Med.*, **21**, 223 (2015).
2. A. Wickia, D. Witzigmannb, V. Balasubramanianc and J. Huwylerb, *J. Control. Release*, **200**, 138 (2015).
3. S. Ummadi, B. Shravani, N. G. R. Rao, M. S. Reddy and B. Nayak, *Int. J. Pharm. Sci.*, **3**, 258 (2013).
4. D. Bhowmik, H. Gopinath, B. Pragati Kumar, S. Duraivel and K. P. Sampath Kumar, *Pharma Innovation.*, **1**, 24 (2012).
5. C. Alvarez-Lorenzo and A. Concheiro, *J. Chromatogr. B.*, **804**, 231 (2004).
6. H. Kempe, A. Parareda Pujolràs and M. Kempe, *Pharm. Res.*, **32**, 375 (2015).
7. M. Ali and M. E. Byrne, *Pharm. Res.*, **26**, 714 (2009).
8. F. Azizi Ishkuh, M. Javanbakht, M. Esfandyari-Manesh, R. Dinarvand and F. Atyabi, *J. Mater. Sci.*, **49**, 6343 (2014).
9. M. E. Byrne, J. Zachary Hilt and N. A. Peppas, *J. Biomed. Mater. Res.*, **84**, 137 (2008).
10. P. Luliski, *Acta Pol. Pharm.*, **70**, 601 (2013).
11. O. Ramstrom and R. J. Ansell, *Chirality*, **10**, 195 (1998).
12. M. Komiyama, T. Takeuchi, T. Mukawa and H. Asanuma, *Molecular Imprinting: From Fundamentals to Applications*, Wiley-VCH, Weinheim (2003).
13. G. Vasapollo, R. Del Sole, L. Mergola, M. R. Lazzoi, A. Scardino, S. Scorrano and G. Mele, *Int. J. Mol. Sci.*, **12**, 5908 (2011).
14. F. Omidi, M. Behbahani, H. Sadeghi Abandansari, A. Sedighi and S. J. Shahtaheri, *J. Environ. Health Sci. Eng.*, **12**, 137 (2014).
15. T. Takeuchia and J. Haginakab, *J. Chromatogr. B.*, **72**, 1 (1999).
16. M. Ulbricht, *J. Chromatogr. B.*, **804**, 113 (2004).
17. L. Uzun and A. Turner, *Biosens. Bioelectron.*, **76**, 131 (2016).
18. J. Xia, X. Cao, Z. Wang, M. Yang, F. Zhang, B. Lu, F. Li, L. Xia, Y. Li and Y. Xia, *Sens. Actuators, B: Chemical.*, **225**, 305 (2016).
19. W. J. Cheong, F. Ali, J. H. Choi, J. O. Lee and K. Y. Sung, *Talanta*, **106**, 45 (2013).

20. J. Lee, S. Bernard and X. Liu, *React. Funct. Polym.*, **69**, 650 (2009).
21. K. Ohkubo, Y. Urata, S. Hirota, Y. Honda, Y. Fujishita and T. Sagawa, *J. Mol. Catal*, **93**, 189 (1994).
22. D. L. Rathbone, *Adv. Drug Deliv. Rev.*, **57**, 1854 (2005).
23. F. Puoci, G. Cirillo, M. Curcio, O. I. Parisi, F. Iemma and N. Picci, *Expert Opin. Drug Deliv.*, **8**, 1379 (2011).
24. B. Sellergren and C. J. Allender, *Adv. Drug Deliv. Rev.*, **57**, 1733 (2005).
25. C. F. van Nostrum, *Drug Discov. Today Technol.*, **2**, 119 (2005).
26. M. S. da Silva, F. L. Nobrega, A. A. Ricardo, E. J. Cabrita and T. Casimiro, *J. Supercrit. Fluids*, **58**, 150 (2011).
27. G. Cirillo, F. Iemma, F. Puoci, O. I. Parisi, M. Curcio, U. G. Spizzirri and N. Picci, *J. Drug Target.*, **17**, 72 (2009).
28. W. Chen, Y. Ma, J. Pan, Z. Meng, G. Pan and B. Sellergren, *Polymers*, **7**, 1689 (2015).
29. D. R. Kryscio and N. A. Peppas, *AIChE J.*, **55**, 1311 (2009).
30. A. Shkilnyy, E. Munnier, K. Herve, M. Souce, R. Benoit, S. Cohen-Jonathan, P. Limelette, M. L. Saboungi, P. Dubois and I. Chourpa, *J. Phys. Chem. C.*, **114**, 5850 (2010).
31. M. Mahmoudi, A. Simchi, M. Imani and U. O. Hafeli, *J. Phys. Chem. C.*, **113**, 8124 (2009).
32. T. Chen, M. I. Shukoor, R. Wang, Z. Zhao, Q. Yuan, S. Bamrungsap, X. Xiong and W. Tan, *ACS Nano.*, **5**, 7866 (2011).
33. P. Dramou, P. Zuo, H. He, L. A. Pham-Huy, w. Zou, D. Xiao, C. Pham-Huyc and T. Ndorbora, *J. Mater. Chem. B.*, **1**, 4099 (2013).
34. O. L. Parisi, C. Morelli, F. Puoci, C. Saturnino, A. Caruso, D. Sisci, G. E. Trombino, N. Piccia and M. S. Sinicropia, *J. Mater. Chem. B.*, **2**, 6619 (2014).
35. X. Kan, Z. Geng, Y. Zhao, Z. Wang and J. J. Zhu, *Nanotechnology*, **20**, 1 (2009).
36. X. Xia, E. P. C. Lai and B. Ormeci, *Polym. Eng. Sci.*, **52**, 1775 (2012).
37. C. Dunn and S. J. Keam, *PharmacoEconomics*, **24**, 495 (2006).
38. D. Simpson, M. P. Curran and C. M. Perry, *Drugs*, **64**, 1213 (2004).
39. J. M. Dixon, C. D. B. Love, C. O. C. Bellamy, D. A. Cameron1, R. C. F. Leonard, H. Smith and W. R. Miller, *Breast Cancer Res Treat.*, **66**, 191 (2001).
40. C. Fontaine, A. Meulemans, M. Huizing, C. Collen, L. Kaufman, J. De Mey, C. Bourgain, G. Verfaillie, J. Lamote, R. Sacre, D. Schallier, B. Neyns, J. Vermorken and J. De Greve, *Breast.*, **17**, 376 (2008).
41. A. Lipton, L. M. Demers, H. A. Harvey, K. B. Kambic, H. Grossberg, C. Brady, H. Adlercruefz, P. F. Trunet and R. J. Sanfen, *Cancer.*, **75**, 2132 (1995).
42. Q. J. Khan, P. S. Reddy, B. F. Kimler, P. Sharma, S. E. Baxa, A. P. O'Dea, J. R. Klemp and C. J. Fabian, *Breast Cancer Res Treat.*, **119**, 111 (2010).
43. S. K. Dey, B. Mandal, M. Bhowmik and L. K. Ghosh, *Braz. J. Pharm. Sci.*, **45**, 585 (2009).
44. A. J. Siddiqa, K. Chaudhury and B. Adhikari, *Colloids Surf., B.*, **116**, 169 (2014).
45. M. R. Saboktakin, R. M. Tabatabaie1, A. Maharramov and M. A. Ramazanov, *J. Pharm. Educ. Res.*, **1**, 62 (2010).
46. S. Kazemi, A. A. Sarabi Daryani, M. Abdouss and Z. Shariatinia, *J. Theor. Comput. Chem.*, **15**, 1650015 (2016).
47. Y. Shi, H. Lv, X. Lu, Y. Huang, Y. Zhanga and W. Xue, *J. Mater. Chem.*, **22**, 3889 (2012).
48. T. Jing, H. Du, Q. Dai, H. Xia, J. Niu, Q. Hao, S. Mei and Y, Zhou, *Biosens. Bioelectron.*, **26**, 301 (2010).
49. Y. Ding, Y. Hu, L. Zhang, Y. Chen and X. Jiang, *Biomacromolecules*, **7**, 1766 (2006).
50. B. Liu, M. Han, G. Guan, S. Wang, R. Liu and Z. Zhang, *J. Phys. Chem. C.*, **115**, 17320 (2011).
51. D. Niu, Z. Zhou, W. Yang, Y. Li, L. Xia, B. Jiang, W. Xu, W. Huang and T. Zhu, *J. Appl. Polym. Sci.*, **130**, 2859 (2013).
52. O. Karaagac, H. Kockar, S. Beyaz and T. Tanrisever, *IEEE Trans. Magn.*, **46**, 3987 (2010).
53. H. Surikumaran, S. Mohamad and N. Muhamad Sarih, *Int. J. Mol. Sci.*, **15**, 6111 (2014).
54. H. G. Schild, *J. Polym. Sci. Part A Polym. Chem.*, **31**, 2403 (1993).
55. Y. Zhang, R. Liu, Y. Hu and G. Li, *Anal. Chem.*, **81**, 967 (2009).
56. A. H. Lu, E. L. Salabas and F. Schuth, *Angew. Chem.*, **46**, 1222 (2007).
57. S. Beyaz, H. Kockar and T. Tanrisever, *J. Optoelectron. Adv. M.*, **1**, 447 (2009).
58. M. Mahdavi, M. Bin Ahmad, J. Haron, F. Namvar, B. Nadi, M. Z. Ab Rahman and J. Amin, *Molecules*, **18**, 7533 (2013).
59. X. X. Li, L. F. Hao, Y. P. Huang, H. Q. Duan and Z. S. Liu, *Polym. Eng. Sci.*, **52**, 1440 (2012).
60. S. Likhitkar and A. K. Bajpai, *Carbohydr. Polym.*, **87**, 300 (2012).
61. N. Griffete, J. Fresnais, A. Espinosa, C. Wilhelm, A. Bée and C. Ménager, *Nanoscale*, **7**, 18891 (2015).
62. G. R. Mahdavinia, H. Etemadi and F. Soleymani, *Carbohydr. Polym.*, **128**, 112 (2015).
63. M. Uva, D. Pasqui, L. Mencuccini, S. Fedi and R. Barbucci, *J. Biomater. Nanobiotechnol.*, **5**, 116 (2014).